PCCP

PAPER

View Article Online
View Journal | View Issue

Cite this: *Phys. Chem. Chem. Phys.*, 2022, **24**, 10193

New opportunities for ultrafast and highly enantio-sensitive imaging of chiral nuclear dynamics enabled by synthetic chiral light†

David Ayuso [ab]

Received 27th November 2021,
Accepted 29th March 2022

DOI: 10.1039/d1cp05427a

rsc.li/pccp

Synthetic chiral light [D. Ayuso *et al.*, *Nat. Photon.*, 2019, **13**, 866–871] has opened up new opportunities for ultrafast and highly efficient imaging and control of chiral matter. Here we show that the giant enantio-sensitivity enabled by such light could be exploited to probe chiral nuclear rearrangements during chemical reactions in a highly enantio-sensitive manner. Using a state-of-the-art implementation of real-time time-dependent density functional theory, we explore how the nonlinear response of the prototypical chiral molecule H_2O_2 changes as a function of its dihedral angle, which defines its handedness. The macroscopic intensity emitted from randomly oriented molecules at even harmonic frequencies (of the fundamental) depends strongly on this nuclear coordinate. Because of the ultrafast nature of such nonlinear interactions, the direct mapping between the dissymmetry factor and the nuclear geometry provides a way to probe chiral nuclear dynamics at their natural time scales. Our work paves the way for ultrafast and highly efficient imaging of enantio-sensitive dynamics in more complex chiral systems, including biologically relevant molecules.

The 21st century has witnessed major advances in the emerging field of attochemistry[1], the goal of which is to visualize and to control the motion of electrons and nuclei during chemical reactions. These include the observation of purely electronic motion in atoms,[2–5] molecules[6–11] and solids,[12–16] as well as of highly correlated dynamics of electrons and nuclei in biologically relevant systems[17], with unprecedented temporal resolution. However, despite these groundbreaking achievements, distinguishing ultrafast left- and right-handed chiral dynamics is still challenging.[18,19]

Chirality plays key roles in a number of scientific areas, from particle physics to pharmacy to astronomy. In general, an object is chiral if it cannot be superimposed to its mirror image. Chiral molecules appear in pairs of left- and right-handed enantiomers. Distinguishing them is vital, *e.g.* because they can present different biological activity.[20] To this goal, we can make them interact with another chiral ''object'', such as chiral light, and measure their enantio-sensitive response.

Well established optical methods for chiral recognition include optical rotation,[21–25] photo-absorption circular dichroism[23–37] and Raman optical activity,[36–39] which address electronic[21–30] and/or vibrational[31–39] degrees of freedom. These techniques rely on weak chiro-optical effects that arise beyond the electric-dipole approximation, posing major challenges for time-resolved measurements of ultrafast chiral dynamics.[18] Developing highly efficient all-optical approaches capable of tracking ultrafast chiral dynamics without relying on weak magnetic interactions is an important challenge that remains unsolved.

More sophisticated chiro-optical methods bypass the need of relying on non-electric–dipole interactions by analyzing enantio-sensitive vectorial observables.[40] In photo-electron circular dichroism (PECD), this vectorial observable is the direction of the photoelectron current upon ionization with circularly polarized light,[41–55] where the forward-backward asymmetry can reach values on the order of 10%. Such a strong enantio-sensitivity has enabled the determination of the enantiomeric excess of mixtures with precision below 1%[50,51] as well as time-resolved measurements of ultrafast chiral dynamics.[52,53] The recent application or tailored two-colour fields to PECD has led to the generation of highly enantio-sensitive tensorial observables.[56–58] However, the total intensity signal in PECD (the total number of emitted photo-electrons) is barely enantio-sensitive, and this method requires angularly resolved measurements.

Using microwave radiation, Patterson and co-workers[59] pioneered a highly efficient way of enantio-discrimination based on purely electric–dipole interactions. More recent achievements include driving enantio-sensitive population transfers between rotational states using fields with three non-coplanar

[a] *Department of Physics, Imperial College London, SW7 2AZ London, UK. E-mail: d.ayuso@imperial.ac.uk*
[b] *Max-Born-Institut, Max-Born-Str. 2A, 12489 Berlin, Germany*

† Electronic supplementary information (ESI) available. See DOI: https://doi.org/10.1039/d1cp05427a

frequency components,[60–62] as well as the development of chiral optical centrifuges[63,64] for enantio-separation. These approaches enable efficient control over the rotational degrees of freedom of chiral molecules in a highly enantio-sensitive way. However, achieving full control over chemical reactions using novel light sources – the ultimate goal of attochemistry – requires acting on the electronic degrees of freedom, on the attosecond to femtosecond time scales.

Synthetic chiral light[65] enables all-optical imaging of chiral matter and ultrafast chiral dynamics at the level of electrons, with extreme enantio-efficiency. Such light is locally chiral: the tip of the electric-field vector draws a chiral, three-dimensional Lissajous figure in time, in every point in space. The enantio-sensitive response of chiral matter to this light arises within the electric–dipole approximation, and is orders of magnitude stronger than in traditional optical methods. We have recently shown that the application of synthetic chiral light[65] to chiral high-harmonic generation can dramatically enhance the enantio-sensitivity of this emerging technique, which so far had relied on the interplay of the chiral molecules with the magnetic component of the light wave.[66–70] We have also shown that the polarization of the driving field can be tailored in time and in space to encode the handedness of a chiral medium in the direction of emission of the harmonic light[71] or in the polarization of the nonlinear response.[72,73]

The giant enantio-sensitivity enabled by synthetic chiral light opens up promising opportunities for ultrafast imaging and control of chiral matter. Can we exploit it to monitor, in real time, the nuclear rearrangements occurring during enantio-sensitive chemical reactions, with high enantio-sensitivity? Here we aim to provide (positive) answer this question.

This paper is organized as follows. First, we review the key aspects of synthetic chiral light, introduced in ref. 65. Second, we describe the numerical method that we have applied to compute ultrafast nonlinear dynamics in the prototypical chiral molecule H_2O_2, which is a convenient model to test our ideas. Third, we show how the enantio-sensitive response of this molecule depends strongly on its nuclear geometry, opening new opportunities for ultrafast imaging of chemical dynamics. We conclude by discussing these opportunities.

1 Synthetic chiral light

The recipe for creating synthetic chiral light[65] has two main ingredients. The first one is related to the multi-colour nature of such fields: we need at least two phase-locked frequencies. Phase locking is key because the handedness of synthetic chiral light is sensitive to the multi-colour phase delays. The second one is a relatively strong longitudinal component, *i.e.* an electric field component in the propagation direction, which is absent in standard light, but appears naturally in non-collinear configurations or tightly focused beams.[74] This longitudinal component allows the Lissajous curve of the field to be three-dimensional and chiral.

Here we use the original configuration of synthetic chiral light, introduced in ref. 65. The proposed optical setup is depicted in Fig. 1. It requires two laser beams that propagate non-collinearly in the xy plane, creating small angles $\pm\alpha$ with respect to the y direction, with propagation vectors

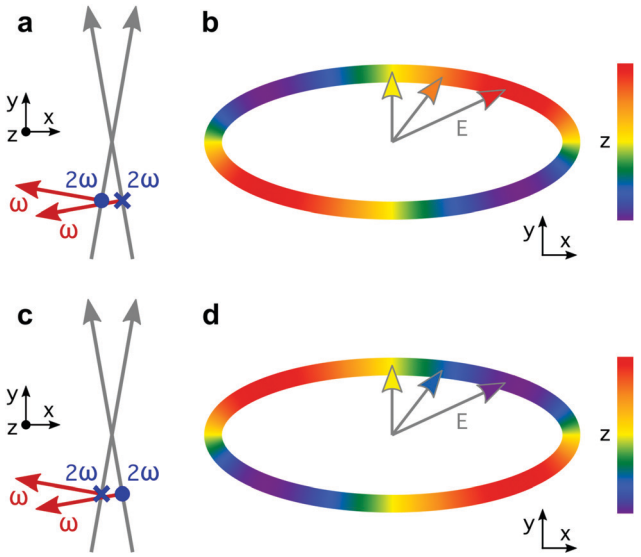

Fig. 1 Synthetic chiral light. (a) A locally and globally chiral field can be created using two laser beams that propagate non-collinearly and carry two cross-polarized colours: the fundamental ω frequency and its second harmonic, with opposite $\omega - 2\omega$ phase delay in the two beams: $\phi_{2\omega}^{(2)} = \phi_{2\omega}^{(1)} + \pi$. (b) Lissajous figure drawn by the tip of the total electric-field vector in the region of overlap between the two beams (c and d). Shifting the two-colour phase delay in the two beams by π is equivalent to reflecting the optical setup on the xy plane (c), and thus it reverses the handedness of the chiral Lissajous figure (d). Note that, because the Lissajous figure that the tip of the electric-field vector draws in time (b and d) is chiral, the enantio-sensitive response of the molecules does not rely on their interaction with the magnetic component of the field (not shown).

$$\mathbf{k}_1 = k\sin(\alpha)\hat{\mathbf{x}} + k\cos(\alpha)\hat{\mathbf{y}}, \quad (1)$$

$$\mathbf{k}_2 = -k\sin(\alpha)\hat{\mathbf{x}} + k\cos(\alpha)\hat{\mathbf{y}}, \quad (2)$$

where $k = 2\pi/\lambda$, with λ being the fundamental wavelength. Both beams carry two orthogonally polarized colours: the fundamental frequency ω, polarized in the xy propagation plane, and its z-polarized second harmonic. Near the focus, the electric-field components of the two laser beams ($n = 1, 2$) can be written as:

$$\mathbf{E}_{\omega}^{(n)}(\mathbf{r}, t) = A_{\omega}^{(n)}(\mathbf{r}, t)\, e^{-\rho_n 2/w2} \cos(\mathbf{k}_n\cdot\mathbf{r} - \omega t)\, \hat{\mathbf{e}}_n, \quad (3)$$

$$\mathbf{E}_{2\omega}^{(n)}(\mathbf{r}, t) = A_{2\omega}^{(n)}(\mathbf{r}, t)\, e^{-\rho_n 2/w2} \cos(2\mathbf{k}_n\cdot\mathbf{r} - 2\omega t - \phi_{\omega}^{(n)})\, \hat{\mathbf{z}}, \quad (4)$$

where ρ_n is the distance to the beam's axis, w is the beam's waist, $A_{\omega}^{(n)}$ and $A_{2\omega}^{(n)}$ are the envelope functions, and the polarization vectors of the ω-field components are defined as:

$$\hat{\mathbf{e}}_1 = \cos(\alpha)\hat{\mathbf{x}} - \sin(\alpha)\hat{\mathbf{y}}, \quad (5)$$

$$\hat{\mathbf{e}}_2 = \cos(\alpha)\hat{\mathbf{x}} + \sin(\alpha)\hat{\mathbf{y}}. \quad (6)$$

In the region of overlap, the combination of the two beams creates a locally chiral field, where the resulting electric-field vector draws a chiral Lissajous figure in time, as depicted in Fig. 1. We set $y = 0$ at the position of the chiral medium. At $z = 0$, where the field intensity maximizes, and for small α, the total

electric-field vector can be written as

$$\mathbf{E}(x,t) = E_\omega(x)a_\omega(t)[\cos(\omega t)\hat{\mathbf{x}} + \varepsilon(x)\sin(\omega t)\hat{\mathbf{y}}] + E_{2\omega}(x)a_{2\omega}(t)\cos(2\omega t + \phi_{2\omega}^{+})\hat{\mathbf{z}}, \quad (7)$$

where a_ω and $a_{2\omega}$ are temporal envelope functions,

$$E_\omega(x) = 2e^{-x2/w2}\cos(\alpha)\cos(k_x x), \quad (8)$$

$$\varepsilon(x) = -\tan(\alpha)\tan(k_x x), \quad (9)$$

$$E_{2\omega}(x) = 2e^{-x2/w2}\cos(2k_x x + \phi_{2\omega}^{-}), \quad (10)$$

with $k_\alpha = k\sin(\alpha)$, and the two-colour phase delays that define the field's local handedness $\phi_{2\omega}^{+}$ and $\phi_{2\omega}^{-}$ are related to the two-colour phase delays in the individual beams (eqn 4) by

$$\phi_{2\omega}^{\pm} = \frac{\phi_{2\omega}^{(2)} \pm \phi_{2\omega}^{(1)}}{2}. \quad (11)$$

Eqn (7) shows that the total electric field is elliptically polarized at frequency ω in the xy plane, with the minor ellipticity component along y, and has a z-polarized 2ω component, creating the chiral Lissajous figure shown in Fig. 1b.

Locally chiral fields can drive strongly enantio-sensitive interactions at the single-molecule-response level, which are controlled and characterized *via* chiral correlation functions, see ref. 65. However, imprinting this microscopic response into the total macroscopic signal requires an additional condition: the field's handedness needs to be maintained in space, at least to certain extent over the interaction region. That is, synthetic chiral light also needs to be globally chiral. In our setup, this condition is fulfilled if $\phi_{2\omega}^{(2)} = \phi_{2\omega}^{(1)} + \pi$, as depicted in Fig. 1a and c. Then, by changing these phase delays synchronously, we can tailor the shape of the chiral Lissajous figure in a way that its handedness is maintained all over the interaction region. In particular, if we change these phase delays by π in both beams (Fig. 1c), we reverse the handedness of the chiral Lissajous figure (Fig. 1d). Synthetic chiral light that is locally and globally chiral enables the highest possible degree of control over the enantio-sensitive response of chiral matter: quenching the response in one molecular enantiomer while enhancing it in its mirror twin.

The proposed experimental setup to create synthetic chiral light with controlled handedness[65] contains a nonlinear barium borate crystal which doubles the frequency of the fundamental beam, creating a second harmonic field with orthogonal polarization. It also includes calcite wedges, which allow us to control the two-colour the phase delay in the two beams independently. The target chiral medium could be in the gas phase or in a liquid microjet[75], and it would be placed before the focus, as it is common in high harmonic generation experiments to favour phase-matching of the short trajectories.

The enantio-sensitive response of isotropic chiral matter to synthetic chiral light relies on the interference between chiral and achiral contributions to light-induced polarization. The multiphoton pathways describing these interactions in the perturbative regime are depicted in Fig. 2. The chiral contribution (Fig. 2a) involves absorption of $2N + 1$ photons from the

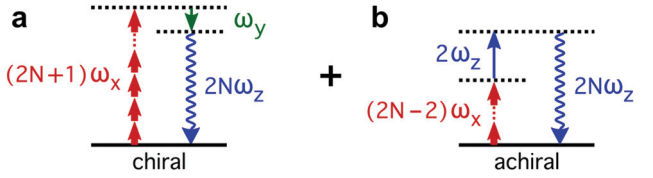

Fig. 2 Multiphoton diagrams describing the enantio-sensitive response of isotropic chiral matter to synthetic chiral light in the perturbative regime. The enantio-sensitive response relies on the interference between two contributions to light-induced polarization: a chiral contribution (a) and an achiral contribution (b), see main text.

(x-polarized) strong-field component and emission of 1 photon into the (y-polarized) weak ellipticity component, leading to polarization at frequency $2N\omega$ along z. This pathway is exclusive of chiral media, and the induced polarization is out of phase in media of opposite handedness. The achiral contribution (Fig. 2b) involves absorption of $2N - 2$ photons from the strong-field component and absorption of 1 photon from the z-polarized 2ω-field, also leading to polarization at frequency $2N\omega$ along z. As these two pathways lead to polarization at the same frequency and along the same axis, they interfere. This interference can be controlled and quantified *via* chiral correlation functions, see ref. 65.

2 Modeling the nonlinear response of H_2O_2 to synthetic chiral light

Hydrogen peroxide constitutes a convenient "toy model" to test the potential of synthetic chiral light as a tool to monitor enantio-sensitive nuclear dynamics in real time. The potential energy curve of the electronic ground state is shown in Fig. 3. It presents a double-well structure, with the two degenerate

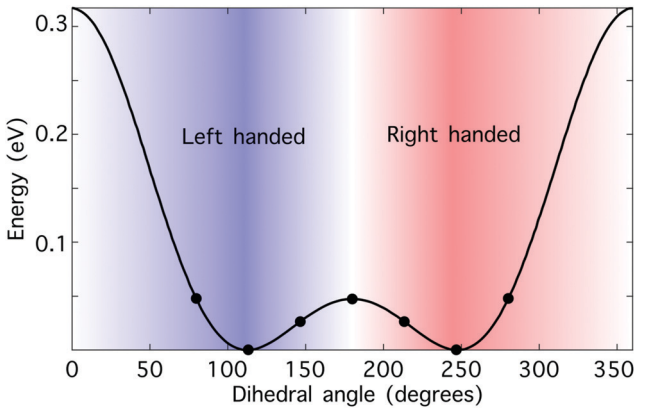

Fig. 3 Hydrogen peroxide as a prototypical chiral molecule with reversible handedness. Potential energy curve of the electronic ground state of H_2O_2 as a function of the dihedral angle β calculated at the B3LYP theory level; the numerical values have been taken from ref. 76. The points indicate the values of the dihedral angle that we have considered in this work. The molecule is achiral if $\beta = 0°$ or $\beta = 180°$, "left-handed" if $0° < \beta < 180°$, and "right-handed" if $180° < \beta < 360°$. The nuclear configurations with dihedral angles β and $360° - \beta$ correspond to molecular enantiomers.

geometries associated with these wells being molecular enantiomers. Indeed, the molecular geometries with dihedral angles β and $360^\circ - \beta$ are mirror twins. However, the energy barrier separating these two wells is small, around 0.5 eV, and thus the two enantiomers coexist in standard conditions. Still, from a computational perspective, the small size of this chiral molecule makes it an ideal candidate to test our ideas.

We have modelled the interaction of H_2O_2 with synthetic chiral light using the state-of-the-art implementation of real-time time-dependent density functional theory in Octopus,[77–80] as described in the ESI.† To describe the physical situation of randomly oriented molecules, we calculated the time-dependent polarization driven by the field in different molecular orientations. The total polarization results from the coherent addition of the contribution from all possible orientations:

$$\mathbf{P}(t,x) = \frac{1}{8\pi^2}\int_0^{2\pi}\int_0^{\pi}\int_0^{2\pi} \mathbf{P}_{\phi\theta\chi}(t,x)\sin(\theta)\mathrm{d}\phi\mathrm{d}\theta\mathrm{d}\chi, \quad (12)$$

where ϕ, θ and χ are the three Euler angles and $\mathbf{P}_{\phi\theta\chi}$ is the polarization response of a particular molecular orientation in the laboratory frame. The polarization is proportional to the time-dependent dipole moment, *i.e.* $\mathbf{P}(t) \propto \langle\Psi(t)|\hat{\mathbf{d}}|\Psi(t)\rangle$. We used the Lebedev quadrature[81] of order 11 to integrate over ϕ and θ, using 50 points to sample the two angles. For each orientation, the laser field was defined in the molecular frame in a way that its strong-field component pointed along $\cos(\phi)\sin(\theta)\mathbf{x}_\mathbf{M} + \sin(\phi)\sin(\theta)\mathbf{y}_\mathbf{M} + \cos(\theta)\mathbf{z}_\mathbf{M}$, where $\mathbf{x}_\mathbf{M}$, $\mathbf{y}_\mathbf{M}$ and $\mathbf{z}_\mathbf{M}$ are the molecular-frame axes. Thus, the orientation of the strong-field component of the laser did not depend on χ, which allowed us to reach convergence using only 4 points in χ in the trapezoidal numerical integration.

We have run numerical simulations for the left-handed configurations of H_2O_2 with dihedral angles 79°, 112° and 146° (see Fig. 3), as described in the ESI.† The results for the opposite right-handed configurations were obtained using symmetry considerations.

In the proposed implementation of synthetic chiral light (see Fig. 1), the longitudinal (y-polarized) component and the 2ω (z-polarized) component are sufficiently weak so the electronic response of the molecules along the y and z directions can be treated perturbatively. That is, the chiral pathway (Fig. 2a) is essentially unaffected by presence of the 2ω field, and the achiral pathway (Fig. 2b) is not modified by the weak ellipticity component. This allowed us to calculate the polarization associated with these pathways separately, see ESI.†

The far-field image was evaluated using the Fraunhofer diffraction equation, as in our previous works.[65,71–73] The amplitude of harmonic emission at a given emission angle κ, or divergence, is given by

$$\tilde{\mathbf{E}}(N\omega,\kappa) \propto \int_{-\infty}^{\infty}[\tilde{P}_x(N\omega,x)\hat{\mathbf{x}} + \tilde{P}_z(N\omega,x)\hat{\mathbf{z}}]\mathrm{e}^{-iN\omega x\kappa/c}\mathrm{d}x, \quad (13)$$

where N is the harmonic number, c is the speed of light in vacuum, and $\tilde{\mathbf{P}} = \tilde{P}_x\hat{\mathbf{x}} + \tilde{P}_y\hat{\mathbf{y}} + \tilde{P}_z\hat{\mathbf{z}}$ is the second derivative of the induced polarization in the frequency domain:

$$\tilde{\mathbf{P}}(N\omega,x) = \int_{-\infty}^{\infty}\frac{\partial^2\mathbf{P}(t,x)}{\partial t^2}\mathrm{e}^{iN\omega t}\mathrm{d}t. \quad (14)$$

That is, the amplitude of harmonic emission is proportional to the rotationally averaged acceleration dipole in the frequency domain[82].

3 Numerical results

We have calculated the highly nonlinear response of different molecular geometries of H_2O_2 to the optical field presented in Fig. 1 using the procedure above described. Symmetry dictates that the enantio-sensitive harmonic signal is completely background free, separated from the non-enantio-sensitive signal in frequency, polarization and space[65]. The non-enantio-sensitive signal appears at odd harmonic frequencies and is polarized along x, whereas the enantio-sensitive response arises at even harmonic frequencies and is polarized along z. They are also emitted in different directions, as shown in our previous work.[65]

Because our field is both locally and globally chiral, the total harmonic intensity, integrated over the emission angle κ, can be strongly enantio-sensitive. The emitted harmonic light has two polarization components which are orthogonal to each other (see eqn (13)), $\tilde{\mathbf{E}} = \tilde{E}_x\hat{\mathbf{x}} + \tilde{E}_z\hat{\mathbf{z}}$. For a better analysis, we decompose the total harmonic intensity into $I = I_x + I_z$, where

$$I_{x/z}(N\omega) \propto \left|\int_{-\pi/2}^{\pi/2}\tilde{E}_{x/z}(N\omega,\kappa)\mathrm{d}\kappa\right|^2. \quad (15)$$

Fig. 4 shows the far-field harmonic intensity emitted by the left- and right-handed equilibrium configurations of H_2O_2. We considered two incident laser beams with fundamental wavelength λ = 400 nm and intensity $I_\omega = 2.5 \times 10^{13}$ W cm^{-2}, so the total intensity in the overlap region reaches 10^{14} W cm^{-2}, and beam waist w = 100 μm. The angle between the propagation directions and the y axis was set to $\alpha = \pm 10^\circ$, the relative field strength of the 2ω-field component was set to $\sqrt{I_{2\omega}/I_\omega} = 0.0125$ in both beams, and the relative phase delays to $\phi_{2\omega}^{(1)} = 0.1\pi$ and $\phi_{2\omega}^{(2)} = 1.1\pi$, so the 2-colour phase delay of the locally chiral field was $\phi_{2\omega}^{+} = 0.6\pi$ (eqn (7)) all over the interaction region.

The non-enantio-sensitive (Fig. 4a) and enantio-sensitive (Fig. 4b) harmonic signals appear at different harmonic orders and are polarized orthogonal to each other, which makes the experimental detection easier. Fig. 4b shows that the enantio-sensitive (z-polarized) intensity emitted from the left- and right-handed enantiomers of H_2O_2 can be dramatically different. Here, we have tuned the relative amplitude and phase of the 2ω-field component to quench emission of harmonic 6 (H6) in the right-handed enantiomer, while maximizing it in the left-handed enantiomer.

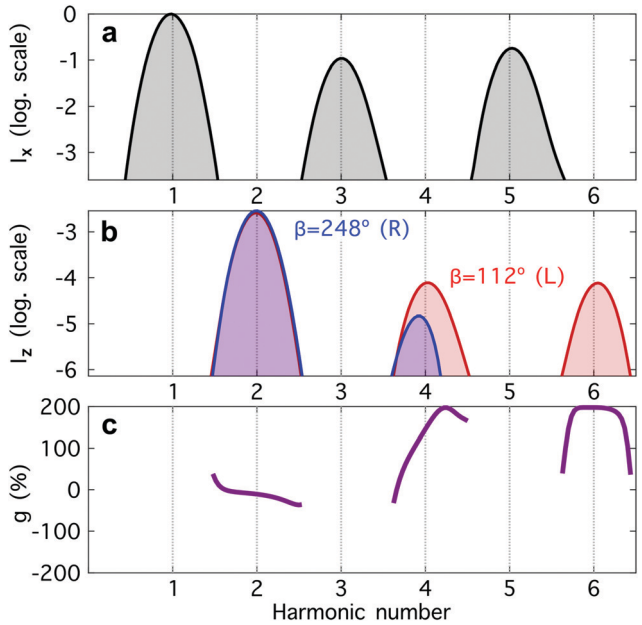

Fig. 4 Harmonic emission from the chiral equilibrium geometries of H_2O_2 driven by synthetic chiral light. (a) Non-enantio-sensitive x-polarized harmonic intensity emitted from the left-handed (β = 112°, see Fig. 3) and right-handed (β = 248°) equilibrium geometries. (b) Enantio-sensitive z-polarized harmonic intensity emitted from the left-handed (β = 112°, red) and right-handed (β = 248°, blue) equilibrium geometries. (c) Dissymmetry factor, see eqn (16). Laser parameters: fundamental wavelength λ = 400 nm, I_ω = 2.5 × 10^{13} W cm^{-2} in each beam, $\sqrt{I_{2\omega}/I_\omega} = 0.0125$, $\alpha = \pm 10°$, $\phi_{2\omega}^{(1)} = 0.1\pi$, $\phi_{2\omega}^{(2)} = 1.1\pi$, and w = 100 μm.

The degree of enantio-sensitivity can be quantified using the dissymmetry factor:

$$g = 2\frac{I_L - I_R}{I_L + I_R}. \quad (16)$$

For the case of H_2O_2, the nuclear configurations with dihedral angles β and $360° - \beta$ are molecular enantiomers, and thus we can easily connect the dissymmetry factor to the molecular geometry *via*

$$I_L = I(\beta), \quad (17)$$

$$I_R = I(360° - \beta), \quad (18)$$

where $0 < \beta < 180°$. In the equilibrium configurations (β = 112°, see Fig. 3), the dissymmetry factor, shown in Fig. 4c, reaches its maximum value of 200%.

An alternative expression of the dissymmetry factor can be defined using the intensity ratio between an enantio-sensitive even (z-polarized) harmonic and a reference odd (x-polarized) harmonic,

$$g' = 2\frac{I_L^{2N}/I_L^{2N+1} - I_R^{2N}/I_R^{2N+1}}{I_L^{2N}/I_L^{2N+1} + I_R^{2N}/I_R^{2N+1}}, \quad (19)$$

rather than absolute intensities (as in eqn (16)). This alternative definition could reduce errors associated with experimental fluctuations in the laser intensity and sample densities. From a theoretical perspective, both definitions are equivalent, as the reference (x-polarized, odd-harmonic intensity) is not enantio-sensitive, *i.e.* $I_L^{2N+1} = I_R^{2N+1}$, and thus $g = g'$.

The enantio-sensitive response of isotropic chiral matter to synthetic chiral light relies on the interference between two contributions to light-induced polarization, as above discussed. The chiral contribution is out of phase in media of opposite handedness and is not affected by the 2ω-field component (Fig. 2a). The achiral contribution is identical in opposite enantiomers, and its intensity and phase can be fully controlled with the relative strength and phase of the 2ω-component of the driving field (Fig. 2b). Thus, by adjusting these parameters, we can achieve perfect constructive interference in one molecular enantiomer and perfect destructive interference the other. As we show in the following, this allows us to reach the limits of the dissymmetry factor (±200%) in any harmonic number and for any nuclear configuration.

Fig. 5 shows the dissymmetry factor for H2, H4 and H6, and for dihedral angles 79°, 112° and 146°, as a function of the relative strength and two-colour phase delay $\phi_{2\omega}^+$, for fixed $\phi_{2\omega}^- = \pi/2$. Note that varying $\phi_{2\omega}^+$ while keeping $\phi_{2\omega}^-$ constant means varying the two-colour delay in the individual beams synchronously, as $\phi_{2\omega}^{(1)} = \phi_{2\omega}^+ - \phi_{2\omega}^-$ and $\phi_{2\omega}^{(2)} = \phi_{2\omega}^+ + \phi_{2\omega}^-$, see eqn (11). By keeping $\phi_{2\omega}^{(2)} - \phi_{2\omega}^{(1)} = \pi$ (*i.e.* $\phi_{2\omega}^- = \pi/2$), we tailor the shape of

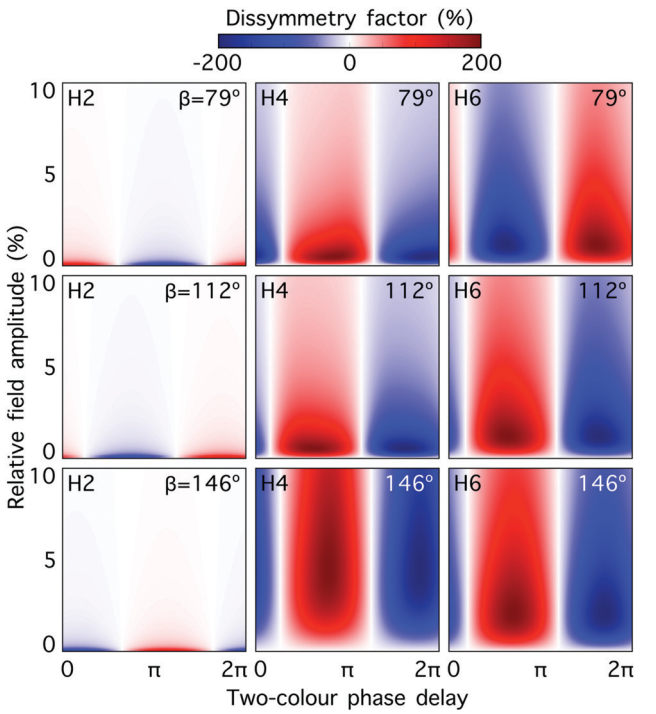

Fig. 5 Dissymmetry factor in the enantio-sensitive z-polarized harmonic intensity emitted from randomly oriented H_2O_2 molecules (see eqn (16)) as a function the two-colour phase delay $\phi_{2\omega}^+$ and relative 2ω-field strength $\sqrt{I_{2\omega}/I_\omega}$, for harmonic numbers 2 (left column), 4 (central column) and 6 (right column), and for dihedral angles 79° (upper row), 112° (central row), 146° (lower row). Here, we vary $\phi_{2\omega}^+$ while keeping $\phi_{2\omega}^- = \pi/2$, *i.e.* we vary the two-colour delay in the individual beams synchronously, as $\phi_{2\omega}^{(1)} = \phi_{2\omega}^+ - \pi/2$ and $\phi_{2\omega}^{(2)} = \phi_{2\omega}^+ + \pi/2$, see eqn (11). This allows us to tailor the shape of the chiral Lissajous figure in a way that its handedness is maintained globally in space.

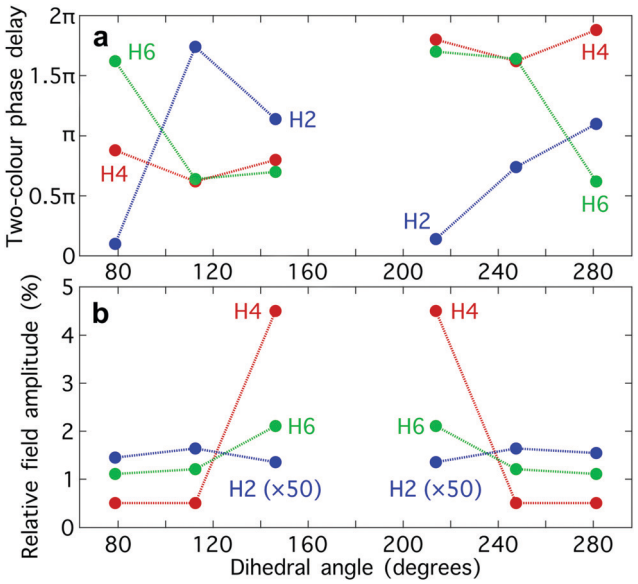

Fig. 6 Maximizing the enantio-sensitive response of hydrogen peroxide. Values of the two-colour phase delay $\phi^{+}_{2\omega}$ (a) and of the relative 2ω-field strength $\sqrt{I_{2\omega}/I_{\omega}}$ (b) which maximize the (z-polarized) enantio-sensitive response of H_2O_2 as functions of the dihedral angle, for harmonic numbers 2 (blue), 4 (red) and 6 (green).

the chiral Lissajous figure in a way that it has the same handedness in every point in space. As already anticipated, the dissymmetry factor reaches the limits of ±200% in all cases. Note that changing $\phi^{+}_{2\omega}$ by π reverses the field's handedness. As a result, the values of $\phi^{+}_{2\omega}$ that maximize the response of the left-handed enantiomer (g = 200%) and the right-handed enantiomer (g = − 200%) are always shifted by π. Furthermore, the phase of the achiral response depends linearly on $\phi^{+}_{2\omega}$ (small variations are due to the shape of the pulse envelope). Thus, the nodal lines in Fig. 5, corresponding to g = 0, are shifted by π/2 with respect to the maximum and the minimum values of g. The specific features of these two-dimensional spectrograms record the nuclear configuration of the molecule.

The optimum values of the relative field strength $\sqrt{I_{2\omega}/I_{\omega}}$ and two-colour phase delay $\phi^{+}_{2\omega}$ which maximize the enantio-sensitive response of the left-handed enantiomer (g = 200% in Fig. 5) are presented in Fig. 6 as functions of the dihedral angle. They are different for each harmonic number, as they are associated with different multiphoton processes. Because the molecular susceptibilities change with the dihedral angle, these optimum parameters are also different for different molecular geometries.

The strong modulation of the two spectroscopic parameters with the dihedral angle reveal that synthetic chiral light is indeed a flexible and powerful spectroscopic tool that allows us to image the nuclear configuration of the molecule in a highly enantio-sensitive manner. Because of the ultrafast nature of the nonlinear interactions responsible for the generation of the enantio-sensitive signal, synthetic chiral light seems to be ideally suited for monitoring chiral chemical reactions in real time.

Conclusions

Monitoring and controlling ultrafast chemical processes at their natural time scales are the ultimate goals of attochemistry. These goals are particularly challenging when dealing with chiral molecules, as the weak non-electric-dipole interactions make the response of left- and right-handed enantiomers to conventional light fields virtually identical. Synthetic chiral light, which is chiral already in the electric dipole approximation, overcomes this fundamental limitation. It creates a new way of imaging and controlling the electronic clouds in chiral molecules with extremely high enantio-sensitivity, introducing new opportunities to this emerging discipline.

Here we have shown that the ultrafast electronic response of the prototypical chiral molecule H_2O_2 is highly sensitive to its nuclear geometry. Despite the simplicity of the molecular system, our numerical results validate the feasibility of synthetic chiral light as a tool for imaging enantio-sensitive chemical reactions in real time, which are ubiquitous in chemistry and of special relevance in biology. Further research should address more complex chiral systems, where synthetic chiral light may allow us to image and control the correlated interplay between electronic and nuclear degrees of freedom, which becomes particularly important in the vicinity of conical intersections.

The possibility of initiating highly enantio-sensitive dynamics in mixtures of left- and right-handed molecules using synthetic chiral light creates interesting opportunities in photo-chemistry, including the possibility of driving enantio-selective photo-chemical reactions.

Conflicts of interest

There are no conflicts to declare.

Acknowledgements

I am extremely grateful to Olga Smirnova and Misha Ivanov for their enormous support and guidance, for pushing me in the right direction, for highly stimulating discussions, and for being a constant source of inspiration. I acknowledge highly stimulating discussions with Andrés F. Ordoñez, expert advice from Oriana Brea in computing the geometry optimizations, and funding from the Royal Society URF\R1\201333 and the Deutsche Forschungsgemeinschaft SPP 1840 SM 292/5-2. I would also like to thank Rose Picciuto and Josh Vogwell for kindly reading the manuscript and providing useful feedback.

References

1 M. Nisoli, *Opt. Photon. News*, 2019, **30**, 32–39.
2 M. Hentschel, R. Kienberger, C. Spielmann, G. A. Reider, N. Milosevic, T. Brabec, P. Corkum, U. Heinzmann, M. Drescher and F. Krausz, *Nature*, 2001, **414**, 509–513.

3 M. Drescher, M. Hentschel, R. Kienberger, M. Uiberacker, V. Yakovlev, A. Scrinzi, T. Westerwalbesloh, U. Kleineberg, U. Heinzmann and F. Krausz, *Nature*, 2002, **419**, 803–807.
4 M. Uiberacker, T. Uphues, M. Schultze, A. J. Verhoef, V. Yakovlev, M. F. Kling, J. Rauschenberger, N. M. Kabachnik, H. Schröder, M. Lezius, K. L. Kompa, H.-G. Muller, M. J. J. Vrakking, S. Hendel, U. Kleineberg, U. Heinzmann, M. Drescher and F. Krausz, *Nature*, 2007, **446**, 627–632.
5 C. Ott, A. Kaldun, L. Argenti, P. Raith, K. Meyer, M. Laux, Y. Zhang, A. Blättermann, S. Hagstotz, T. Ding, R. Heck, J. Madroñero, F. Martín and T. Pfeifer, *Nature*, 2014, **516**, 374–378.
6 F. Martn, J. Fernández, T. Havermeier, L. Foucar, T. Weber, K. Kreidi, M. Schöffler, L. Schmidt, T. Jahnke, O. Jagutzki, A. Czasch, E. P. Benis, T. Osipov, A. L. Landers, A. Belkacem, M. H. Prior, H. Schmidt-Böcking, C. L. Cocke and R. Dörner, *Science*, 2007, **315**, 629–633.
7 O. Smirnova, Y. Mairesse, S. Patchkovskii, N. Dudovich, D. Villeneuve, P. Corkum and M. Y. Ivanov, *Nature*, 2009, **460**, 972–977.
8 G. Sansone, F. Kelkensberg, J. F. Pérez-Torres, F. Morales, M. F. Kling, W. Siu, O. Ghafur, P. Johnsson, M. Swoboda, E. Benedetti, F. Ferrari, F. Lépine, J. L. Sanz-Vicario, S. Zherebtsov, I. Znakovskaya, A. L'Huillier, M. Y. Ivanov, M. Nisoli, F. Martín and M. J. J. Vrakking, *Nature*, 2010, **465**, 763–766.
9 H. J. Wörner, J. B. Bertrand, D. V. Kartashov, P. B. Corkum and D. M. Villeneuve, *Nature*, 2010, **466**, 604–607.
10 F. Calegari, D. Ayuso, A. Trabattoni, L. Belshaw, S. De Camillis, S. Anumula, F. Frassetto, L. Poletto, A. Palacios, P. Decleva, J. B. Greenwood, F. Martn and M. Nisoli, *Science*, 2014, **346**, 336–339.
11 P. Peng, C. Marceau and D. M. Villeneuve, *Nat. Rev. Phys.*, 2019, **1**, 144–155.
12 A. L. Cavalieri, N. Müller, T. Uphues, V. S. Yakovlev, A. Baltuška, B. Horvath, B. Schmidt, L. Blümel, R. Holzwarth, S. Hendel, M. Drescher, U. Kleineberg, P. M. Echenique, R. Kienberger, F. Krausz and U. Heinzmann, *Nature*, 2007, **449**, 1029–1032.
13 M. Schultze, K. Ramasesha, C. Pemmaraju, S. Sato, D. Whitmore, A. Gandman, J. S. Prell, L. J. Borja, D. Prendergast, K. Yabana, D. M. Neumark and S. R. Leone, *Science*, 2014, **346**, 1348–1352.
14 T. T. Luu, M. Garg, S. Y. Kruchinin, A. Moulet, M. T. Hassan and E. Goulielmakis, *Nature*, 2015, **521**, 498–502.
15 Z. Tao, C. Chen, T. Szilvási, M. Keller, M. Mavrikakis, H. Kapteyn and M. Murnane, *Science*, 2016, **353**, 62–67.
16 A. J. Uzan, G. Orenstein, Á. Jiménez-Galán, C. McDonald, R. E. F. Silva, B. D. Bruner, N. D. Klimkin, V. Blanchet, T. Arusi-Parpar, M. Krüger, A. N. Rubtsov, O. Smirnova, M. Ivanov, B. Yan, T. Brabec and N. Dudovich, *Nat. Photonics*, 2020, **14**, 183–187.
17 D. Polli, P. Altoè, O. Weingart, K. M. Spillane, C. Manzoni, D. Brida, G. Tomasello, G. Orlandi, P. Kukura, R. A. Mathies, M. Garavelli and G. Cerullo, *Nature*, 2010, **467**, 440–443.
18 M. Oppermann, J. Spekowius, B. Bauer, R. Pfister, M. Chergui and J. Helbing, *J. Phys. Chem. Lett.*, 2019, **10**, 2700–2705.
19 M. Schmid, L. Martinez-Fernandez, D. Markovitsi, F. Santoro, F. Hache, R. Improta and P. Changenet, *J. Phys. Chem. Lett.*, 2019, **10**, 4089–4094.
20 D. J. Abraham, T. J. Hagen and T. R. Helgren, Chirality and Drug Discovery, in *Burger's Medicinal Chemistry and Drug Discovery*, ed. D. J. Abraham, 2022.
21 P. L. Polavarapu and D. K. Chakraborty, *J. Am. Chem. Soc.*, 1998, **120**, 6160–6164.
22 P. Stephens, D. McCann, J. Cheeseman and M. Frisch, *Chirality*, 2005, **17**, S52–S64.
23 J. A. Schellman, *Chem. Rev.*, 1975, **75**, 323–331.
24 D. M. McCann and P. J. Stephens, *J. Org. Chem.*, 2006, **71**, 6074–6098.
25 T. D. Crawford, M. C. Tam and M. L. Abrams, *J. Phys. Chem. A*, 2007, **111**, 12057–12068.
26 F. Pulm, J. Schramm, J. Hormes, S. Grimme and S. D. Peyerimhoff, *Chem. Phys.*, 1997, **224**, 143–155.
27 N. Berova, L. D. Bari and G. Pescitelli, *Chem. Soc. Rev.*, 2007, **36**, 914–931.
28 C. Toro, L. De Boni, N. Lin, F. Santoro, A. Rizzo and F. Hernandez, *Chem. – Eur. J.*, 2010, **16**, 3504–3509.
29 G. Pescitelli, L. Di Bari and N. Berova, *Chem. Soc. Rev.*, 2011, **40**, 4603–4625.
30 C. Wolf and K. W. Bentley, *Chem. Soc. Rev.*, 2013, **42**, 5408–5424.
31 L. A. Nafie, T. A. Keiderling and P. J. Stephens, *J. Am. Chem. Soc.*, 1976, **98**, 2715–2723.
32 T. A. Keiderling, *Appl. Spectrosc. Rev.*, 1981, **17**, 189–226.
33 P. J. Stephens, *J. Phys. Chem.*, 1985, **89**, 748–752.
34 T. B. Freedman, X. Cao, R. K. Dukor and L. A. Nafie, *Chirality*, 2003, **15**, 743–758.
35 I. Dolamic, B. Varnholt and T. Bürgi, *Nat. Commun.*, 2015, **6**, 7117.
36 J. M. Batista Jr., E. W. Blanch and V. d. S. Bolzani, *Nat. Prod. Rep.*, 2015, **32**, 1280–1302.
37 L. D. Barron and A. D. Buckingham, *Chem. Phys. Lett.*, 2010, **492**, 199–213.
38 J. Haesler, I. Schindelholz, E. Riguet, C. G. Bochet and W. Hug, *Nature*, 2007, **446**, 526–529.
39 Y. He, B. Wang, R. K. Dukor and L. A. Nafie, *Appl. Spectrosc.*, 2011, **65**, 699–723.
40 A. F. Ordonez and O. Smirnova, *Phys. Rev. A*, 2018, **98**, 063428.
41 B. Ritchie, *Phys. Rev. A*, 1976, **13**, 1411–1415.
42 I. Powis, *J. Chem. Phys.*, 2000, **112**, 301–310.
43 N. Böwering, T. Lischke, B. Schmidtke, N. Müller, T. Khalil and U. Heinzmann, *Phys. Rev. Lett.*, 2001, **86**, 1187–1190.
44 G. A. Garcia, L. Nahon, M. Lebech, J.-C. Houver, D. Dowek and I. Powis, *J. Chem. Phys.*, 2003, **119**, 8781–8784.
45 C. Lux, M. Wollenhaupt, T. Bolze, Q. Liang, J. Köhler, C. Sarpe and T. Baumert, *Angew. Chem., Int. Ed.*, 2012, **51**, 5001–5005.
46 C. S. Lehmann, N. B. Ram, I. Powis and M. H. M. Janssen, *J. Chem. Phys.*, 2013, **139**, 234307.

47 G. A. Garcia, L. Nahon, S. Daly and I. Powis, *Nat. Commun.*, 2013, **4**, 2132.
48 M. H. M. Janssen and I. Powis, *Phys. Chem. Chem. Phys.*, 2014, **16**, 856–871.
49 C. Lux, M. Wollenhaupt, C. Sarpe and T. Baumert, *ChemPhysChem*, 2015, **16**, 115–137.
50 A. Kastner, C. Lux, T. Ring, S. Züllighoven, C. Sarpe, A. Senftleben and T. Baumert, *ChemPhysChem*, 2016, **17**, 1119–1122.
51 A. Comby, E. Bloch, C. M. M. Bond, D. Descamps, J. Miles, S. Petit, S. Rozen, J. B. Greenwood, V. Blanchet and Y. Mairesse, *Nat. Commun.*, 2018, **9**, 5212.
52 A. Comby, S. Beaulieu, M. Boggio-Pasqua, D. Descamps, F. Légaré, L. Nahon, S. Petit, B. Pons, B. Fabre, Y. Mairesse and V. Blanchet, *J. Phys. Chem. Lett.*, 2016, **7**, 4514–4519.
53 S. Beaulieu, A. Comby, B. Fabre, D. Descamps, A. Ferré, G. Garcia, R. Géneaux, F. Légaré, L. Nahon, S. Petit, T. Ruchon, B. Pons, V. Blanchet and Y. Mairesse, *Faraday Discuss.*, 2016, **194**, 325–348.
54 S. Beaulieu, A. Comby, A. Clergerie, J. Caillat, D. Descamps, N. Dudovich, B. Fabre, R. Géneaux, F. Légaré, S. Petit, B. Pons, G. Porat, T. Ruchon, R. Taeb, V. Blanchet and Y. Mairesse, *Science*, 2017, **358**, 1288–1294.
55 S. Beaulieu, A. Comby, D. Descamps, B. Fabre, G. A. Garcia, R. Géneaux, A. G. Harvey, F. Légaré, Z. Masín, L. Nahon, A. F. Ordonez, S. Petit, B. Pons, Y. Mairesse, O. Smirnova and V. Blanchet, *Nat. Phys.*, 2018, **14**, 484–489.
56 P. V. Demekhin, A. N. Artemyev, A. Kastner and T. Baumert, *Phys. Rev. Lett.*, 2018, **121**, 253201.
57 R. E. Goetz, C. P. Koch and L. Greenman, *Phys. Rev. Lett.*, 2019, **122**, 013204.
58 S. Rozen, A. Comby, E. Bloch, S. Beauvarlet, D. Descamps, B. Fabre, S. Petit, V. Blanchet, B. Pons, N. Dudovich and Y. Mairesse, *Phys. Rev. X*, 2019, **9**, 031004.
59 D. Patterson, M. Schnell and J. M. Doyle, *Nature*, 2013, **497**, 475–477.
60 S. Eibenberger, J. Doyle and D. Patterson, *Phys. Rev. Lett.*, 2017, **118**, 123002.
61 V. A. Shubert, D. Schmitz, C. Pérez, C. Medcraft, A. Krin, S. R. Domingos, D. Patterson and M. Schnell, *J. Phys. Chem. Lett.*, 2016, **7**, 341–350.
62 C. Pérez, A. L. Steber, S. R. Domingos, A. Krin, D. Schmitz and M. Schnell, *Angew. Chem., Int. Ed.*, 2017, **56**, 12512–12517.
63 A. Yachmenev, J. Onvlee, E. Zak, A. Owens and J. Küpper, *Phys. Rev. Lett.*, 2019, **123**, 243202.
64 A. A. Milner, J. A. M. Fordyce, I. MacPhail-Bartley, W. Wasserman, V. Milner, I. Tutunnikov and I. S. Averbukh, *Phys. Rev. Lett.*, 2019, **122**, 223201.
65 D. Ayuso, O. Neufeld, A. F. Ordonez, P. Decleva, G. Lerner, O. Cohen, M. Ivanov and O. Smirnova, *Nat. Photonics*, 2019, **13**, 866–871.
66 R. Cireasa, A. E. Boguslavskiy, B. Pons, M. C. H. Wong, D. Descamps, S. Petit, H. Ruf, N. Thiré, A. Ferré, J. Suarez, J. Higuet, B. E. Schmidt, A. F. Alharbi, F. Légaré, V. Blanchet, B. Fabre, S. Patchkovskii, O. Smirnova, Y. Mairesse and V. R. Bhardwaj, *Nat. Phys.*, 2015, **11**, 654–658.
67 D. Ayuso, P. Decleva, S. Patchkowskii and O. Smirnova, *J. Phys. B: At., Mol. Opt. Phys.*, 2018, **51**, 06LT01.
68 D. Ayuso, P. Decleva, S. Patchkowskii and O. Smirnova, *J. Phys. B: At., Mol. Opt. Phys.*, 2018, **51**, 124002.
69 Y. Harada, E. Haraguchi, K. Kaneshima and T. Sekikawa, *Phys. Rev. A*, 2018, **98**, 021401.
70 D. Baykusheva and H. J. Wörner, *Phys. Rev. X*, 2018, **8**, 031060.
71 D. Ayuso, A. F. Ordonez, P. Decleva, M. Ivanov and O. Smirnova, *Nat. Commun.*, 2021, **12**, 3951.
72 O. Neufeld, D. Ayuso, P. Decleva, M. Y. Ivanov, O. Smirnova and O. Cohen, *Phys. Rev. X*, 2019, **9**, 031002.
73 D. Ayuso, A. F. Ordonez, M. Ivanov and O. Smirnova, *Optica*, 2021, **8**, 1243–1246.
74 K. Y. Bliokh and F. Nori, *Phys. Rep.*, 2015, **592**, 1–38.
75 G. Galinis, J. Strucka, J. C. T. Barnard, A. Braun, R. A. Smith and J. P. Marangos, *Rev. Sci. Instrum.*, 2017, **88**, 083117.
76 U. Kuenzer and T. S. Hofer, *Chem. Phys. Lett.*, 2019, **728**, 195–200.
77 M. A. Marques, A. Castro, G. F. Bertsch and A. Rubio, *Comput. Phys. Commun.*, 2003, **151**, 60–78.
78 A. Castro, H. Appel, M. Oliveira, C. A. Rozzi, X. Andrade, F. Lorenzen, M. A. L. Marques, E. K. U. Gross and A. Rubio, *Phys. Status Solidi B*, 2006, **243**, 2465–2488.
79 X. Andrade, D. Strubbe, U. De Giovannini, A. H. Larsen, M. J. T. Oliveira, J. Alberdi-Rodriguez, A. Varas, I. Theophilou, N. Helbig, M. J. Verstraete, L. Stella, F. Nogueira, A. Aspuru-Gzik, A. Castro, M. A. L. Marques and A. Rubio, *Phys. Chem. Chem. Phys.*, 2015, **17**, 31371–31396.
80 N. Tancogne-Dejean, M. J. T. Oliveira, X. Andrade, H. Appel, C. H. Borca, G. Le Breton, F. Buchholz, A. Castro, S. Corni, A. A. Correa, U. De Giovannini, A. Delgado, F. G. Eich, J. Flick, G. Gil, A. Gomez, N. Helbig, H. Hübener, R. Jestädt, J. Jornet-Somoza, A. H. Larsen, I. V. Lebedeva, M. Lüders, M. A. L. Marques, S. T. Ohlmann, S. Pipolo, M. Rampp, C. A. Rozzi, D. A. Strubbe, S. A. Sato, C. Schäfer, I. Theophilou, A. Welden and A. Rubio, *J. Chem. Phys.*, 2020, **152**, 124119.
81 V. I. Lebedev and D. N. Laikov, *Doklady Mathematics*, 1999, **59**, 477–481.
82 O. Smirnova and M. Ivanov, *Multielectron High Harmonic Generation: Simple Man on a Complex Plane*, John Wiley & Sons, Ltd, 2014, ch. 7, pp. 201–256.